ON THE RADIO AND OPTICAL LUMINOSITY EVOLUTION OF QUASARS

J. SINGAL¹, V. PETROSIAN^{1,2}, A. LAWRENCE³, L. STAWARZ^{4,5}

ABSTRACT

We calculate simultaneously the radio and optical luminosity evolutions of quasars, and the distribution in radio loudness R defined as the ratio of radio and optical luminosities, using a flux limited data set containing 636 quasars with radio and optical fluxes from White et al. We first note that when dealing with multivariate data it is imperative to first determine the true correlations among the variables, not those introduced by the observational selection effects, before obtaining the individual distributions of the variables. We use the methods developed by Efron and Petrosian which are designed to obtain unbiased correlations, distributions, and evolution with redshift from a data set truncated due to observational biases. It is found that as expected the population of quasars exhibits strong positive correlation between the radio and optical luminosities and that this correlation deviates from a simple linear relation in a way indicating that more luminous quasars are more radio loud. We also find that there is a strong luminosity evolution with redshift in both wavebands, with significantly higher radio than optical evolution. We conclude that the luminosity evolution obtained by arbitrarily separating the sources into radio loud (R > 10) and radio quiet (R < 10) populations introduces significant biases that skew the result considerably. We also construct the local radio and optical luminosity functions and the density evolution. Finally, we consider the distribution of the radio loudness parameter R obtained from careful treatment of the selection effects and luminosity evolutions with that obtained from the raw data without such considerations. We find a significant difference between the two distributions and no clear sign of bi-modality in the true distribution. Our results indicate therefore, somewhat surprisingly, that there is no critical switch in the efficiency of the production of disk outflows/jets between very radio quiet and very radio loud quasars, but rather a smooth transition. Also, this efficiency seems higher for the high-redshift and more luminous sources in the considered sample.

Subject headings: quasars: general - methods: data analysis - methods: statistical - galaxies: active - galaxies: jets - galaxies: luminosity function

1. INTRODUCTION

The optical emission of quasar sources is dominated by the radiation of the plasma accreting onto supermassive black holes, while the radio emission is dominated by the plasma outflowing from the black hole/accretion disk systems. Hence different but complementary information can be gathered in both photon energy ranges regarding the cosmological evolution of active galactic nuclei (AGN) and its relation to structure formation in the Universe. It is therefore important to analyze in detail redshift distributions of quasar sources in both frequency regimes, investigating carefully any possible differences between these two.

The rapid evolution of quasars identified in radio catalogs as 'quasi-stellar radio sources' (or QSRs) in the redshift range $z \leq 2$ was established soon after their discovery (e.g. Schmidt 1967). Subsequent optical discoveries of similar sources, most of which had no detectable radio emission, lead to the emergence of the class of 'radio quiet quasars' (or 'quasi-stellar objects'; QSOs for short e.g. Osterbrock (1989)). These optically-selected sources also showed similar strong evolutionary trends, similar to the radio-selected ones. These evolutions are interpreted as density evolution, luminosity evolution or a combination of the two in numerous works (e.g. Schmidt 1967; Petrosian 1973; Marshall et al. 1983; Dunlop & Peacock 1990; Maloney & Petrosian 1999; Willott et al. 2001) and can be designated as the evolution of the luminosity function (LF, for short).

By now the evolution of the LF has been described not only for optical and radio luminosities but also for X-ray, infrared, and bolometric luminosities (e.g. Ueda et al. 2003; Richards et al. 2006; Matute et al. 2006; Hopkins et al. 2007; Croom et al. 2009). Most of these studies have treated the evolution with a bi-variate function $\Psi_i(L_i, z)$, where L_i is the luminosity (or luminosity spectral density) in some photon energy range, e.g. $L_i = L_{opt}$ or L_{rad} . The shape of the LF and its evolution are usually obtained from a flux limited sample $f_i > f_{m,i}$ with $L_i = 4 \pi d_L(z)^2 K_i(z) f_i$, where d_L is the luminosity distance and $K_i(z)$ stands for the K-correction. For a power law emission spectrum of index ε_i defined as $f_i \propto \nu^{\varepsilon_i}$, one has $K_i(z) = (1+z)^{1+\varepsilon_i}$.

However, because no matter how a quasar is discovered, optical observations are required for determination of redshift, then the flux limit of optical observations

jsingal@stanford.edu

¹ Kavli Institute for Particle Astrophysics and Cosmology SLAC National Accelerator Laboratory and Stanford University 382 Via Pueblo Mall, Stanford, CA 94305-4060

² Also Departments of Physics and Applied Physics

³ University of Edinburgh Institute for Astronomy

Scottish Universities Physics Alliance (SUPA)

Royal Observatory, Blackford Hill, Edinburgh UK ⁴ Institute of Space and Astronautical Science (ISAS)

Japan Aerospace Exploration Agency (JAXA),

³⁻¹⁻¹ Yoshinodai, Chuo-ku, Sagamihara, Kanagawa 252-5510 Japan ⁵ Astronomical observatory of the Jagiellonian University

⁵Astronomical observatory of the Jagiellonian University ul. Orla 171, 30-244 Kraków, Poland

 $(f_{m,opt})$ and the optical luminosity enter the picture, so that one now must consider the joint (tri-variate) LF and its evolution $\Psi(L_{opt}, L_i, z)$, with $L_i = L_{rad}$ or L_X , for example.

In general, the first step required for investigation of a multivariate distribution is the determination of whether the variables of the distributions are correlated or are statistically independent. For example, in the case of a single luminosity function the correlation between Land z is what we call luminosity evolution, and independence of these variables would imply absence of luminosity evolution. Mathematically, independence means that the function is separable $\Psi_i(L_i, z) = \psi_i(L_i) \times \rho(z)$, in which case one is left with the determination of a single variable LF $\psi_i(L_i)$ and the density evolution $\rho(z)$. As shown by Petrosian (1992) the most exact nonparametric method for this task from a flux limited (or a more generally truncated) sample is the Lynden-Bell (1971) method. However, this simple and elegant method cannot be used for cases when variables are correlated (e.g. when there is luminosity evolution). Efron & Petrosian (1992, 1999) (EP for short) developed new methods for determination of the existence of correlation or independence of the variables from a flux limited and more generally truncated data set, and prescribed how to remove the correlation by defining new and independent variables [say $L'_i \equiv L'_i/g_i(z)$ and z, where the function $g_i(z)$ describes the luminosity evolution] and then how to determine the mono-variate functions $\psi_i(L'_i)$ and $\rho(z)$. Thus, one can determine both the luminosity and density evolutions $g_i(z)$ and $\rho(z)$, as well as the LF at any redshift.⁶

In the case of quasars with the optical and some other band luminosity, we have at least a tri-variate function. In this case one must determine not only the correlations between the redshift and individual luminosities (i.e. the two luminosity evolutions) but also the possible correlation between the two luminosities, before individual distributions can be determined. Knowledge of these correlations and distributions are essential for not only constraining robustly the cosmological evolution of active galaxies, but also for interpretation of related observations, such as the extragalactic background radiation (e.g. Singal et al. 2010; Hopkins et al. 2010).

Another related aspect of this subject, which has attracted considerable attention over the years, is the distinction between so-called 'radio loud' and 'radio quiet' quasars. No observations have been presented so far providing conclusive evidence that both types of objects belong to very different populations of sources, or, equivalently, that the quasar family is characterized by a bi-modal distribution in this respect; (cf Ivezic et al. 2002; Cirasuolo et al. 2003), nor that the relative fraction of radio loud/quiet quasars evolves with redshift (Goldschmidt et al. 1999; Jiang et al. 2007). The question of whether there are two distinct populations was addressed soon after the discovery of quasars using small samples with radio flux limits greater than one Jy. It was shown then that the distribution of the ratio of ra-

dio to optical luminosity $R \equiv L_{rad}/L_{opt}$, the so called "radio loudness parameter", was not bi-modal but was a fairly broad $(2.8 < \log R < 5.2)$ power law with index $\beta_R \sim -2.3$ (Schmidt 1972; Petrosian 1973). At that time this ratio was defined for the radio luminosity at $\nu_{rad} = 0.5$ GHz and optical luminosity at 2500 Å (or the frequency $\nu_{opt} = 1.2 \times 10^{15}$ Hz). Nowadays it is defined with radio luminosity at 5 GHz so that for a mean radio spectral index $\varepsilon_{rad} \sim -0.6$ the old data would be in the range 2.2 to 4.6 of the modern definition of $R.^7$ Moreover, the survey limits have been extended to much lower fluxes (specially in the radio domain), and this resulted in a much wider range of the ratio that extends to values well below one, namely $-3 < \log R < 5$. In addition, hints of the bi-modality of the distribution suggested that $\log R = 1$ could be chosen as the radio loud/quiet demarcation value (Kellerman et al. 1989).

There have been many papers dealing with this ratio and radio loud vs radio quiet issue, as well as luminosity ratios at other wavelengths, e.g. IR/radio, Optical/Xray etc. However, none of these works have dealt with the distribution (and/or evolution) of the ratio, which is related to the tri-variate LF $\Psi(L_{opt}, L_{rad}, z)$ by⁸

$$G_R(R,z) = \int_0^\infty \Psi(L_{opt}, R \ L_{opt}, z) \ L_{opt} \ dL_{opt}$$
$$= \int_0^\infty \Psi\left(\frac{L_{rad}}{R}, L_{rad}, z\right) \ L_{rad} \ \frac{dL_{rad}}{R^2}$$
(1)

These works did not take the observational selection effects properly into consideration, nor did they address the correlations between the radio and optical luminosities. Neglecting these effects when attempting to determine the distribution of radio loudness is usually given the justification that the ratio is essentially independent of cosmological model and redshift (as long as the Kcorrections are the same). The distribution of observed ratios obtained in this way (see Figure 14 below) is really broad and deviates from a simple power law and may even have a hint of bi-modality, seemingly justifying at face value the choice of $\log R = 1$ as the separation point between radio loud and quiest sources. However, as shown in the Appendix even in the simplest cases the observed distribution (and its moments) could be very different from the intrinsic ones, and can even show artificial bi-modality. Thus, for determination of the true distribution of R the data truncations must be determined and the correlations between all variables must be properly evaluated.

Our aim in this paper is to take all these effects into account in determination of the evolution of optical and radio luminosities and their ratio and to find their distributions, with particular emphasis on the radio loudness

 $^{^{6}}$ It should be noted that here we assume that the shape of the luminosity function is constant; e.g. power law indices describing the LF are independent of z. In general, shape variations can affect the test of independence. For a sufficiently large sample the importance of these effects can be determined and accounted for. This is beyond the scope of this paper.

⁷ The fiducial cosmological model used at that time, namely the Einstein-De Sitter model, was also different than the currently accelerating models. However, this will effect the values of the individual luminosities but not the ratio R. We also note that some other authors use B-band optical fluxes in defining the radio loudness parameter, but the difference is not large, resulting in a change in the ratio of radio to optical luminosities by a factor of 1.33, for the assumed optical spectral index $\varepsilon_{opt} = -0.5$.

⁸ Equation 1 arises because by definition $\int G_R(R, z) dR = \int \int \Psi(L_{opt}, L_{rad} z) dL_{opt} dL_{rad}$, and from the definition of R, $dL_{rad} = L_{opt} dR$ and $dL_{opt} = -(L_{rad}/R^2) dR$.

question. In §2 we describe the data we use. In §3 we provide an overview of the procedure used for determination of simultaneous luminosity functions, luminosity evolution, and density evolution, and the notation used. In §4 we describe how we obtain the luminosity evolution and other correlations, and present our results on the evolution of the LFs. In §5 we describe the density evolution and the luminosity density evolutions, while in §6 we calculate the LF corrected for luminosity evolution, which we call the "local" LF. Finally, in §7 we evaluate the distribution of radio loudness, R. This work assumes the standard Λ CDM cosmology throughout, with $H_0 = 71 \,\mathrm{km\,s^{-1}\,Mpc^{-1}}$, $\Omega_{\Lambda} = 0.7$ and $\Omega_m = 0.3$.

2. DATASET

In order to evaluate the luminosity evolution in both radio and optical, and to separate and compare these effects, we require a data set that has both radio and optical fluxes to reasonable limits and across a range of redshifts, that contains a significant number of both radio loud (RL) and radio quiet (RQ) objects. The overlap of the FIRST bright guasar radio survey with the Automatic Plate Measuring Facility catalog of the Palomar Observatory Sky Survey (POSS-I), as presented by White et al. (2000), is such a data set. It contains 636 objects with optical R band optical magnitudes, 1.4 GHz total and peak pixel fluxes, and spectroscopic redshifts. The survey has a limiting R band magnitude of 17.8 or $f_{m,R} = 0.22$ mJy, a limiting peak pixel 1.4 GHz flux of 1 mJy, and redshifts that range from 0.02 to 3.425. Figures 1 and 2 show the radio and optical luminosities versus redshifts of the quasars in the survey, assuming the standard K-corrections for power laws with indices $\varepsilon_{opt} = -0.5$ and and $\varepsilon_{rad} = -0.6$ for optical and radio respectively. Figure 3 shows the radio loudness parameter \bar{R} versus redshift for the dataset.

This sample spans a very wide range of luminosities (5 dex in optical and 7 dex in radio) with a significant number of sources in the range $0.1 < R < 10^4$ (with 244 radio loud and 392 radio quiet). Therefore, it is well suited for our analysis here. We have examined some other combined radio and optical survey data sets and found them to be not as well suited for this analysis. For example, the combined FIRST radio survey with the 2dF optical survey as reported in Cirasuolo et al. (2003) features only 12 radio quiet objects (of 113 total), and the combined FIRST with the Large Bright Quasar Survey (LBQS) as reported in Hewett et al. (2001) has only 77 objects and different optical flux limits for the various fields, making the method employed here cumbersome.

3. GENERAL REMARKS ON CORRELATIONS IN LUMINOSITY FUNCTIONS

The luminosity function gives the number of objects per unit comoving volume V per unit source luminosity, so that the cumulative number density is $dN/dV = \int dL_i \Psi_i(L_i, z)$. To examine luminosity evolution, without loss of generality, we can write a LF in some waveband *i* as

$$\Psi_i(L_i, z) = \rho(z) \,\psi_i(L_i/g_i(z), \eta_i^j)/g_i(z), \qquad (2)$$

where $g_i(z)$ and $\rho(z)$ describe the luminosity evolution and comoving object density evolution with redshift respectively and η_i^j stands for parameters that describe the

FIG. 1.— The 2500 Å rest frame absolute luminosity density for the quasars in the White et al. (2000) dataset used in this analysis. To obtain the 2500 Å luminosity we first convert R band magnitude to a flux, and then to a luminosity based on the luminosity distance obtained from the redshift and the standard cosmology. We then assume a -0.5 optical spectral index to K-correct to the rest-frame luminosity at the R band integrated center, and finally scale by the -0.5 optical spectral index to 2500 Å. The crosses are the 'radio loud' objects while the diamonds are the 'radio quiet'.

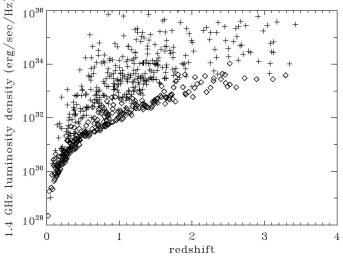
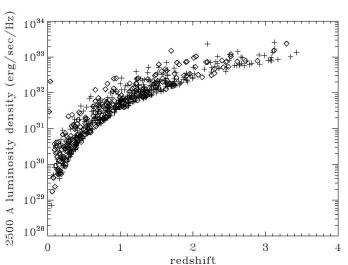


FIG. 2.— The 1.4 GHz rest frame absolute luminosity density for the quasars in the White et al. (2000) dataset used in this analysis. To obtain the 1.4 GHz luminosity density we convert from flux density to luminosity density based on the luminosity distance obtained from the redshift and the standard cosmology, then assume a -0.6 radio spectral index to K-correct to rest frame 1.4 GHz luminosity density. The crosses are the 'radio loud' objects while the diamonds are the 'radio quiet'.

shape (e.g. power law indices and break values) of the *i* band LF (we use the normalization $\int_0^\infty \psi_i(L_i)dL_i = 1$).⁹ In what follows we assume a non-evolving shape for the LF (i.e. $\eta_j = \text{const}$, independent of *L* and *z*), which is a good approximation for determining the global evolutions. Once these are determined this hypothesis can



 $^{^9}$ There are in principle other possible parameters, e.g. the spectral indices. We can ignore them for the purposes of the analysis here on the assumption that they either do not evolve strongly with redshift *or* are not strongly correlated with any of the luminosities in question.

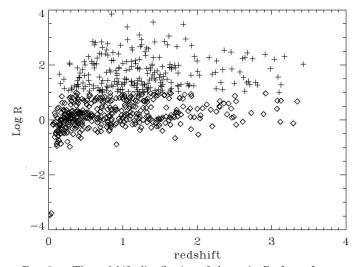


FIG. 3.— The redshift distribution of the ratio R of rest frame absolute luminosities at 5 GHz and 2500 Å for the quasars in the White et al. (2000) dataset used in this analysis. The 5 GHz luminosity is obtained assuming a radio spectral index of -0.6. The crosses are the 'radio loud' objects while the diamonds are the 'radio quiet'.

be tested and results amended. However, for more complicated functional forms with variable η_i^j , e.g. for luminosity dependent density evolution, the determination of the variations will require a large sample with significant numbers of objects in reasonably narrow redshift and radio loudness bins.

Given this assumption then once the luminosity evolution $g_i(z)$ is calculated, the density evolution $\rho(z)$ and local luminosity function $\psi_i(L'_i) \equiv \psi_i(L_i/g_i(z))/g_i(z)$ can be determined.¹⁰ We consider this form of the luminosity function for luminosities in different bands, allowing for separate (optical and radio) luminosity evolution.

1. As is often done, one might naively assume that the joint LF $\Psi(L_{opt}, L_{rad}, z)$ is separable into two forms like equation 2 with a common density evolution. However, as discussed in §1, because the optical and radio luminosities of the quasars are, in general, highly correlated, the simultaneous determination of the luminosity functions of both requires care. The first step in this procedure should be to determine the degree and form of the correlation between the optical and radio luminosities. As described below, the EP method allows us to determine whether any pair of variables are independent or correlated. Once it is determined that they are correlated one should seek a coordinate transformation to define a new pair of variables which are independent. This requires a parametric form for the transformation. One can define a new luminosity which is a combination of the two; we can define a "correlation reduced tion of the two; we can define a correlation reduced radio luminosity" $L_{crr} = L_{rad}/F(L_{opt}/L_{fid})$, where the function F describes the correlation between L_{rad} and L_{opt} and L_{fid} is a fiducial luminosity taken here to be $10^{28} \,\mathrm{erg \, sec^{-1} \, Hz^{-1}}$. This is a convenient choice for L_{fid} as it is lower than the lowest 2500 Å luminosity considered in our sample, but results do not depend on the

particular choice of numerical value. For the correlation function we will assume a simple power law

$$L_{crr} = \frac{L_{rad}}{(L_{opt}/L_{fid})^{\alpha}} \tag{3}$$

where α is a bulk power law correlation index to be determined by a fit to the data (expected to be close to unity because of the strong correlation between the luminosities). This is essentially a coordinate rotation in the log-log luminosity space. As shown in §4 below, EP also prescribe a method to determine a best fit value for the index α which orthogonalizes the new luminosities. Given the correlation function we can then transform the data (and its truncation) into the new independent pair of luminosities (L_{opt} and L_{crr}), whose distribution can be represented as

$$\Psi(L_{opt}, L_{crr}, z) = \rho(z) \times \psi_{opt}(L_{opt}/g_{opt}, \eta_{opt,j})/g_{opt} \times \psi_{crr}(L_{crr}/g_{crr}, \eta_{crr,j})/g_{crr}.$$
(4)

2. The next step is determination of the two *independent* luminosity-redshift correlation functions g_{opt} and g_{crr} which describe the luminosity evolutions. The procedure for determination of these functions is similar to the ones for removing the correlations between the luminosities except now we make coordinate transformations in the $L_{opt} - z$ and $L_{crr} - z$ spaces. We assume simple forms

$$g_i(z) = (1+z)^{k_i}$$
(5)

so that $L'_i = L_i/g_i(z)$ refer to the local (z = 0) luminosities.¹¹ The full procedure is detailed in §4.

3. The density evolution function $\rho(z)$ is determined by the method shown in EP (see §5 below). Once all correlations are removed we end up with a local separable LF as in equation 4.

4. The local LFs of uncorrelated luminosities L'_{opt} and L'_{crr} can then be used to recover the local radio LF by a straight forward integration over L'_{crr} and the true local optical LF as

$$\psi_{rad}(L'_{rad}) = \int_0^\infty \psi_{opt}(L'_{opt}) \,\psi_{crr} \left(\frac{L'_{rad}}{(L'_{opt}/L_{fid})^\alpha}\right) \,\frac{dL'_{opt}}{(L'_{opt}/L_{fid})^\alpha} \,(6)$$

As stated above this procedure can be used for the determination of the radio LF at any redshift, from which one can deduce that the radio luminosities also undergo luminosity evolution with

$$g_{rad}(z) = g_{crr}(z) \times [g_{opt}(z)]^{\alpha}$$
(7)

(cf equation 3)

5. Similarly we can determine the local distribution of the radio to optical luminosity ratio, $R' = L'_{rad}/L'_{opt} = L'_{crr} \times L'_{opt} {}^{\alpha-1} \times L_{fid} {}^{-\alpha}$, as

 11 This is an arbitrary choice. One can chose any other fiducial redshift by defining $g_i(z)=[(1+z)/(1+z_{fid})]^{k_i}.$

¹⁰ The method developed by EP that we shall use below actually gives the cumulative functions $\sigma(< z) = \int_0^z \dot{\rho}(z') \left[dV(z')/dz' \right] dz'$ and $\phi(>L') = \int_{L'}^\infty \psi(L'') dL''$. The differential functions ρ and ψ are obtained by differentiation.

$$G_{R'} = \int_0^\infty \psi_{opt}(L'_{opt}) \,\psi_{crr} \left(\frac{R' \,L_{fid}}{(L'_{opt}/L_{fid})^{\alpha-1}}\right) \,\frac{dL'_{opt}}{L'_{opt}^{\alpha-1} L_{fid}}$$
(8)

and its evolution

$$g_R(z) = g_{crr}(z) \times [g_{opt}(z)]^{\alpha - 1} = \frac{g_{rad}}{g_{opt}}$$
(9)

4. CORRELATION FUNCTIONS

We now describe results obtained from the use of the procedures described in §3 on the data described in §2. Here we first give a brief summary of the algebra involved in the EP method. We follow closely the steps described in Maloney & Petrosian (1999). This method uses the Spearman rank test to determine the best-fit values of parameters describing the correlation functions using the test statistic

$$\tau = \frac{\sum_{j} \left(R_j - E_j \right)}{\sqrt{\sum_{j} V_j}} \tag{10}$$

to test the independence of two variables in a data set, say (x_j, y_j) for $j = 1, \ldots, n$. Here R_j is the y rank of the data point j in a set associated with it. For a untruncated data (i.e. data truncated parallel to the axes) the associated set of point j includes all of the $x_k < x_j$. If the data is truncated, rather than including in equation 10 for each j all points of lower x value in evaluating the y rank, one must form the associated set consisting only of those points of lower x value that would have been observed if they were at the x value of point j given the truncation. As an example, if the truncations apply to the y values of the data and are such that $y_j^+ = \infty$ but y_j^- varies with each x_j , then the associated set $A_j = \{k : y_k > y_j, y_k^- < y_j\}$ (see EP for a full discussion of this method).

If (x_j, y_j) were independent then the rank R_j should be distributed uniformly between 0 and 1 with the expectation value and variance $E_j = (1/2)(j+1)$ and $V_j = (1/12)(j^2+1)$, respectively. Independence is rejected at the $n\sigma$ level if $|\tau| > n$. To find the best fit correlation the y data are then adjusted by defining $y'_j = y_j/F(x_j)$ and the rank test is repeated, with different values of parameters of the function F.

4.1. Radio-Optical Luminosity Correlation

The radio and optical luminosities are obtained from radio and optical fluxes from a two flux limited sample so that the data points in the two dimensional flux space are truncated parallel to the axes which we consider to be untruncated. Since the two luminosities have essentially the same relationship with their respective fluxes, except for a minor difference in the K-correction terms, we can consider the luminosity data to also be untruncated. In that case as mentioned above the determination of the associated set is trivial and one is dealing with the standard Spearman rank test. Assuming the correlation function between the luminosities $F(x) = x^{\alpha}$ we calculate the test statistic τ as a function of α . Figure 4 shows the absolute value of the τ vs α , from which we get the best fit value of $\alpha = 1.4$ with one σ range +0.1

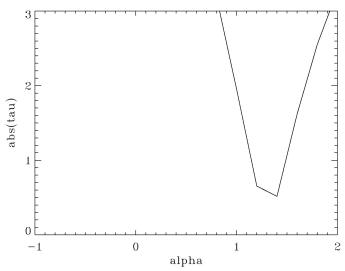


FIG. 4.— The absolute value of the τ statistic as given by equation 10 as a function of α for the relation $L_{rad} \propto (L_{opt})^{\alpha}$, where L_{opt} and L_{rad} are the optical and radio luminosities, respectively, for the quasars in the dataset. The 1 σ range for the best fit value of α is where $|\tau| \leq 1$.

and -0.2. As expected α is near unity but the fact that it deviates from unity is important. It means that the raido loudness increases with luminosity.

4.2. Luminosity-Redshift Correlations

We now describe our results on determination of the luminosity evolution, i.e. the luminosity-redshift correlation functions $g_i(z)$, which according to equation 5 reduces to determination of the values of the index k_i . The basic method for determining the best fit k_i is the same as above but in this case the procedure is more complicated for several reasons. First, as evident from Figures 1 and 2 the $L_i - z$ data are heavily truncated due to the flux limits. Second, we now are dealing with a three dimensional distribution (L_{crr}, L_{opt}, z) and two correlation functions $[g_{crr}(z)$ and $g_{opt}(z)]$.

Specifically, since we have two criteria for truncation, the associated set for each object includes only those objects that are sufficiently luminous in both bands to exceed both flux minima for inclusion in the survey if they were located at the redshift of the object in question. Consequently, we have a two dimensional minimization problem, because both the optical and correlation reduced radio evolution factors, $g_{opt}(z) = (1+z)^{k_{opt}}$ and $g_{crr}(z) = (1+z)^{k_{crr}}$, come into play, as the luminosity cutoff limits for a given redshift are adjusted by powers of k_{opt} and k_{rad} too.

We form a test statistic $\tau_{comb} = \sqrt{\tau_{opt}^2 + \tau_{crr}^2}$ where τ_{opt} and τ_{crr} are those evaluated considering the objects' optical and correlation reduced radio luminosities, respectively. The favored values of k_{opt} and k_{crr} are those that simultaneously give the lowest τ_{comb} and, again, we take the 1σ limits as those in which $\tau_{comb} < 1$. For visualization, Figure 5 shows a surface plot of τ_{comb}

We have verified this method with a simulated Monte Carlo data set in which objects are distributed in redshift and given randomized luminosities in accordance with set optical and radio evolutions. The algorithm can recover the evolutions correctly provided that they aren't wildly different, i.e. one very positive and the other very

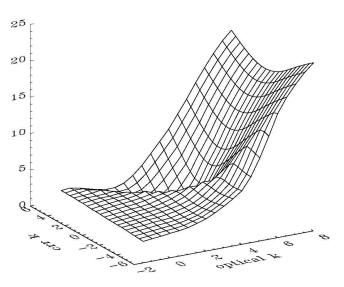


FIG. 5.— Surface plot of the value of τ_{comb} for the dataset as a whole showing the location of the minimum region where the favored values of k_{opt} and k_{crr} lie.

negative.

Figure 6 shows the optical and correlation reduced radio luminosity evolution indices, using the functional forms $g_{opt}(z) = (1 + z)^{k_{opt}}$ and $g_{crr}(z) = (1 + z)^{k_{crr}}$ and taking the contours for 1 and 2 σ about the minimum τ_{comb} . Results are shown for the entire dataset taken as a whole, and also with the data split into the RL and RQ subsets. The radio luminosity evolution itself can be recovered by equation 7.

Given the tight constraints achieved when the dataset is considered as a whole, and the sharp bifurcation when the set is split into the RL and RQ populations, it is evident that splitting the population before determination of the luminosity evolutions introduces a bias into the determinations. This is expected because differing evolutions will have a strong effect on whether an object will continue to be RL or RQ according to the standard definition used here, and the data for each set will be artificially truncated along R = 10 as a function of the evolutions.

We see that positive evolution in both radio and optical wavebands is favored. The minimum value of τ_{comb} favors an optical evolution of $k_{opt} = 4.0$ and a radio evolution of $k_{rad} = 6.6$, but uncertainty at the 1σ level allows the range of k_{opt} from 3.25 to 4.25, and k_{rad} from 6.1 to 7.0. Therefore, we conclude that quasars have undergone a significantly greater radio evolution relative to optical evolution with redshift.

5. DENSITY EVOLUTION

Next we determine the density evolution $\rho(z)$. One can define the cumulative density function

$$\sigma(z) = \int_0^z \rho(z) \, dz \tag{11}$$

and, following Petrosian (1992) based on Lynden-Bell (1971), $\sigma(z)$ can be calculated by

$$\sigma(z) = \prod_{j} \left(1 + \frac{1}{m(j)} \right) \tag{12}$$

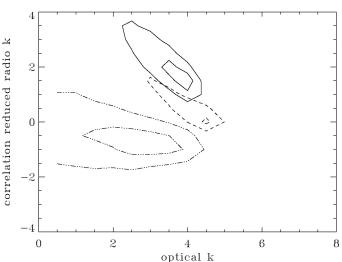


FIG. 6.— The 1σ and 2σ contours for the simultaneous values of k_{opt} and k_{crr} where the optical and correlation reduced radio luminosity evolutions are $g_{opt}(z) = (1+z)^{k_{opt}}$ and $g_{crr}(z) = (1+z)^{k_{crr}}$. The radio luminosity evolution can be reconstructed from $g_{rad} = g_{crr} \times g_{opt}^{1.4}$. Results are shown for the data set evaluated as a whole (solid contours), and for the radio loud (dash-dot contours) and radio quiet (dashed contours) populations evaluated separately. It is evident that splitting the population before determination of the luminosity evolutions introduces a bias into the determinations, as discussed in §4.2.

where j runs over all objects with a redshift lower than or equal to z, and m(j) is the number of objects with a redshift lower than the redshift of object j which are in object j's associated set. In this case, the associated set is again those objects with sufficient optical and radio luminosity that they would be seen if they were at object j's redshift. The use of only the associated set for each object removes the biases introduced by the data truncation. Then the density evolution $\rho(z)$ is

$$\rho(z) = \frac{d\sigma(z)}{dz} \tag{13}$$

However, to determine the density evolution, the previously determined (in §4) luminosity evolution must be taken out. Thus, the objects' optical and radio luminosities, as well as the optical and radio luminosity for inclusion in the associated set for given redshifts, are scaled by taking out factors of $g_{opt}(z) = (1+z)^{k_{opt}}$ and $g_{rad}(z) = (1+z)^{k_{rad}}$, with k_{opt} and k_{rad} determined as above.

Figures 7 and 8 show $\sigma(z)$ and $\rho(z)$ for the objects in the data set. We evaluate and display the density evolution separately for the radio loud and radio quiet objects and for the dataset as a whole to compare them. It is seen that the two groups, divided in this way, exhibit very similar density evolution. The number density of quasars seems to peak at between redshifts 1 and 1.5, a little earlier than generally thought for the most luminous quasars (e.g. Shaver et al. 1996) but similar to the peak found for less luminous quasars by Hopkins et al. (2007), and in agreement with Maloney & Petrosian (1999).

Knowing both the luminosity evolutions $g_i(z)$, and the density evolution $\rho(z)$, one can form the luminosity density functions $\mathcal{L}_i(z)$, which are the total rate of production of energy of quasars as a function of redshift. We show this for the radio luminosity density $\mathcal{L}_{rad}(z)$. As

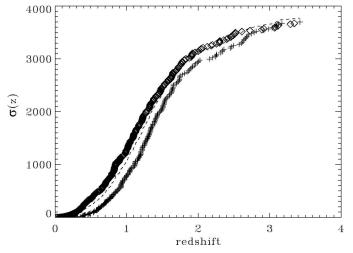


FIG. 7.— The cumulative density function $\sigma(z)$ vs. redshift for the RL (crosses) RQ (diamonds) and all (dashed line) quasars in the data set. The normalization of $\sigma(z)$ is arbitrary, and the RL data has been shifted vertically for clarity. A piecewise quadratic fit to $\sigma(z)$ is used to determine $\rho(z)$ by equation 13.

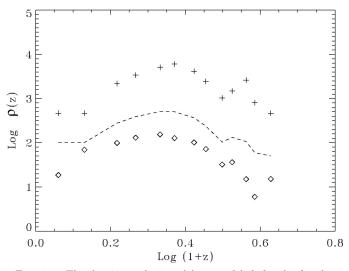


FIG. 8.— The density evolution $\rho(z)$ vs. redshift for the for the RL (crosses) RQ (diamonds) and all (dashed line) quasars in the data set, shown with customary log scales. The normalization of $\rho(z)$ is arbitrary and the curves have been shifted vertically for clarity.

evident the two populations of RL and RQ have very similar shape of radio luminosity density functions (Figure 9)

6. LOCAL LUMINOSITY FUNCTIONS

6.1. General Considerations

In a parallel procedure we can use the 'local' (redshift evolution taken out, or 'de-evolved') luminosity L'_i distributions (and de-evolved luminosity thresholds) to determine the 'local' luminosity functions $\psi_i(L'_i)$, where again the *i* represents the waveband, and the prime indicates that the luminosity evolution has been taken out. We first obtain the cumulative luminosity function

$$\Phi_i(L'_i) = \int_{L'}^{\infty} \psi_i(L''_i) \, dL''_i \tag{14}$$

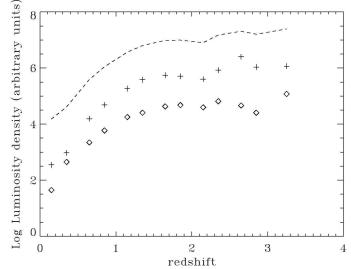


FIG. 9.— The radio luminosity density function $\pounds_{rad}(z)$ vs. redshift for the for the RL (crosses) RQ (diamonds) and all (dashed line) quasars in the data set. The normalization of $\pounds_{rad}(z)$ is arbitrary, and the values have been shifted vertically for clarity. It is seen that the two populations have very similar luminosity density evolution with redshift.

and, following Petrosian (1992), $\Phi_i(L'_i)$ can be calculated by

$$\Phi_i(L'_i) = \prod_k \left(1 + \frac{1}{n(k)}\right)$$
(15)

where k runs over all objects with a luminosity greater than or equal to L_i , and n(k) is the number of objects with a luminosity higher than the luminosity of object k which are in object k's associated set, determined in the same manner as above. The luminosity function $\psi_i(L'_i)$ is

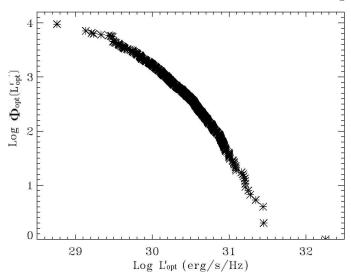
$$\psi_i(L'_i) = -\frac{d\Phi_i(L'_i)}{dL'_i} \tag{16}$$

In §4 we have determined the luminosity evolution for two independent functions, the optical luminosity L_{opt} and the correlation reduced radio luminosity L_{crr} . We can form the local optical $\psi_{opt}(L'_{opt})$ and correlation reduced radio $\psi_{crr}(L'_{crr})$ luminosity functions straightforwardly, by taking the evolutions out. As before, the objects' luminosities, as well as the luminosity limits for inclusion in the associated set for given redshifts, are scaled by taking out factors of $g_{crr}(z) = (1+z)^{k_{crr}}$ and $g_{opt}(z) = (1+z)^{k_{opt}}$, with k_{crr} and k_{opt} determined in §4. We use the notation $L \to L' \equiv L/g(z)$.

6.2. Local optical luminosity function

Figures 10 and 11 show the local cumulative $\Phi_{opt}(L'_{opt})$ and differential $\psi_{opt}(L'_{opt})$ local optical LFs of the quasars in the White et al. (2000) dataset, while figure 12 shows the local correlation reduced radio LF, $\psi_{crr}(L'_{crr})$.

The optical LF shows evidence of a break at 2×10^{30} erg sec⁻¹ Hz⁻¹, which was present already in data used in Petrosian (1973). Fitting a broken power law yields values -1.3 ± 0.1 and -3.0 ± 0.1 below and above the break, respectively. As the optical luminosity function has been studied extensively in various AGN sur-



8

FIG. 10.— The cumulative local optical luminosity function $\Phi_{opt}(L'_{opt})$ for the quasars in the data set. A piecewise quadratic fit to $\Phi(L'_{opt})$ is used to determine $\psi_{opt}(L'_{opt})$ by equation 16.

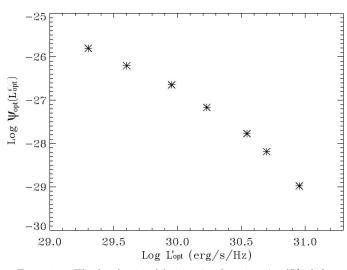


FIG. 11.— The local optical luminosity function $\psi_{opt}(L'_{opt})$ for the quasars in the data set.

veys, we can compare the slope of $\psi_{opt}(L'_{opt})$ obtained here to values reported in the literature. For example, Boyle et al. (2000), using the 2dF optical data set (but with no radio overlap criteria) use a customary broken power law form for the luminosity function, with values ranging from -1.39 to -3.95 for different realizations, showing reasonable agreement¹²

6.3. Local radio luminosity function

With $\psi_{opt}(L'_{opt})$ and $\psi_{crr}(L'_{crr})$, we can determine the local radio luminosity function $\psi_{rad}(L'_{rad})$ with equation 6. Figure 13 shows the local radio luminosity function $\psi_{rad}(L'_{rad})$ reconstructed in this way. It is seen that the local radio luminosity function contains a possible break around $10^{31} \text{ erg sec}^{-1} \text{ Hz}^{-1}$, with a power law slope of -1.5 ± 0.1 below the break and -2.5 ± 0.1 above

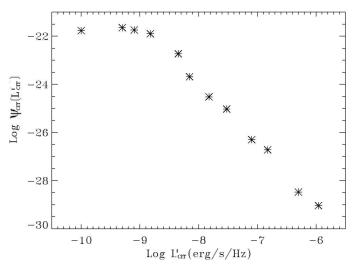


FIG. 12.— The local correlation reduced radio luminosity function $\psi_{crr}(L'_{crr})$ for the quasars in the data set.

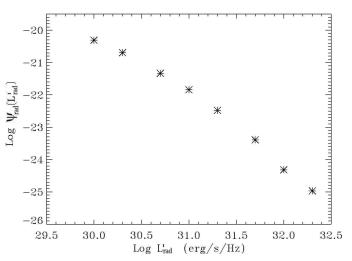


FIG. 13.— The local radio luminosity function $\psi_{rad}(L'_{rad})$ for the quasars in the data set.

it. The slope above the break seen here is similar to earlier results of Schmidt (1972) and Petrosian (1973) which probed only those luminosities. A more complete comparison can be made with Mauch & Sadler (2007), who form radio luminosity functions of local sources in the Second Incremental Data Release of the 6 degree Field Galaxy Survey (2dFGRS) radio catalog. For the sources they identify as AGN, they find a break at $3.1 \times 10^{31} \,\mathrm{erg \, sec^{-1} \, Hz^{-1}}$, with slopes of -2.27 ± 0.18 and -1.49 ± 0.04 above and below the break (converting to luminosity units).

7. DISTRIBUTION OF RADIO LOUDNESS RATIOS

As stated in the introduction, naively one may expect that because the ratio R is independent of cosmological model and nearly independent of redshift, the raw observed distribution would provide a good representation of the true distribution of this ratio. In Figure 14 we show this raw distribution by the triangles, arrived at by using the raw values of R from the data and forming a distribution in the manner of equations 15 and 16 with no data truncations. It appears that this naive approach shows a hint of possible bi-modality with $\log R = 1$ as the

 $^{^{12}}$ It should be noted that they parameterize evolution differently and work in absolute magnitudes rather than luminosities, however the slopes of their fits to the LF as they parameterize it are applicable, as can be seen in their section 3.2.2.

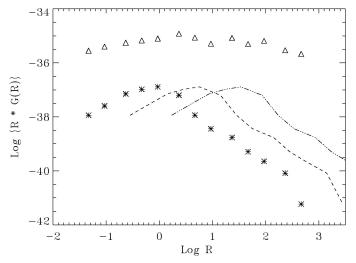


FIG. 14.— The local distribution $G_R(R)$ in the 5 GHz radio to 2500 Å optical luminosity ratio R, plotted as $R \times G_R(R)$, for the quasars in the data set. The stars are from $G_{R'}(R')$ as determined by the method of Equation 8, taking account of the truncations and correlations in the luminosity evolutions, while the triangles result from forming a distribution with a naive use of the objects' raw ratio. The normalization is arbitrary and the curves have been shifted vertically for clarity. It is seen that the naive method gives a hint of a bi-modal distribution, while the proper method does not. Also shown is the proper radio loudness distribution $G_R(R, z)$ at redshifts z=1 (dashed line) and z=3 (dash-dot line), evolved according to the form of equation 9.

dividing value.¹³ However, as shown in the Appendix the raw distribution can be far from the true distribution and selection biases can introduce a false bi-modality.

As discussed in §3, we can reconstruct the local distribution of $G_{R'}(R')$, as in Equation 8, which provides for a more proper accounting of the biases and truncations. The results of this calculation are also shown in Figure 14. The distribution calculated in this way clearly is different than the raw distribution, and does not show an apparent bi-modality. There is still a possible feature in the same region (logR = 1) where the raw distribution shows a dip. This feature is of marginal significance and results from the similarly shaped feature in $\psi_{crr}(L'_{crr})$ centered around $L'_{crr} = 10^{-8} \text{ erg sec}^{-1} \text{ Hz}^{-1}$. Even if significant, this change in slope cannot be taken as evidence for two physically distinct populations, but could be a useful point to make an arbitrary division into radio loud and radio quiet objects. We also note that R = 1 is apparently the most probable value for the radio loudness.

We also know the redshift evolution of the ratio, given equation 9, is $g_R(z) = (1+z)^{2.6}$. The effect on the distribution of R is also shown in Figure 14. Another way to look at this is that we have found that the radio luminosity evolves at a different rate than the optical luminosity, with the consequence that their ratio is a function of redshift. The radio loudness of the population increases by a factor of 6 by redshift 1, and by a factor of 37 by redshift 3. Other works have noted that the fraction of radio loud quasars may increase with redshift. Miller et al. (1990) compare the radio loud fraction at different redshifts and find significant positive evolution in the fraction of radio loud objects. However, they attribute this to an effect of there being two populations (RL and RQ) that evolve differently. Donoso et al. (2009) compute radio and optical luminosity functions at different redshifts and reach the same conclusion. We note that our results favor one population, in the sense that the distribution of G(R), recovered from considering the data truncations inherent in the survey and correlations between the luminosities, is continuous.

8. TESTS OF ASSUMPTIONS

One may raise the concern that the simple power law parameterization used for the redshift luminosity evolutions (equation 5) may not be the most ideal one. In particular, it may not accurately represent the evolutions at the highest redshifts considered here. To check this, we repeat the analysis with a different parameterization for the luminosity evolution which allows for a flattening at higher redshifts,

$$g_i(z) = \frac{(1+z)^{k_i}}{1+(\frac{1+z}{4})^{k_i}},\tag{17}$$

where *i* again represents the optical or correlation reduced radio luminosity. In this parameterization, the functional form for the radio luminosity evolution $g_{rad}(z)$ and the evolution of the radio loudness parameter $g_R(z)$ are lengthier experssions involving $k_{opt} k_{crr}$ and α , given equations 7 and 9.

This alternate parameterization for the evolutions does not appreciably effect the results. The best fit evolution factors as a function of redshift under the alternate parameterization differ very little from those in the simple parameterization to redshift 3.5 (the highest object in the sample).

Another concern may be that luminosity dependent density evolution (LDDE), which is not considered in the functional forms for the LF used here, may more accurately represent the evolution of the LF. As a check of this effect, we divide the data into high and low luminosity halves (cutting on optical luminosity), and check the similarity of the computed density evolutions for the two sets versus that computed assuming the absence of LDDE. Given that an artificial difference is already introduced in the two halves because there are a lack of low luminosity objects in the high redshift sample and a lack of high luminosity redshifts in the low redshift sample (see Figures 1 and 2), we conclude that the density evolutions determined in this way are sufficiently similar to justify neglecting LDDE.

9. DISCUSSION

We have used a general and robust method to determine the radio and optical luminosity evolutions simultaneously for the quasars in the White et al. (2000) dataset, which combines 1.4 GHz radio and R-band optical data for 636 quasars ranging in redshifts from 0.02 to 3.425 and over seven orders of magnitude in radio loudness. We find that the quasars exhibit more substantial radio evolution than optical evolution with redshift (§4.2 and Figure 6). We also show that when divided into radio loud (RL) and radio quiet (RQ) sets accordingly to the standard definition (divided by the value of the radioloudness parameter R = 10), the two sub-populations exhibit similar density evolution. The local optical and

 $^{^{13}}$ We note that in general apparent bi-modalities often do not stand up to rigorous statistical tests.

radio luminosity functions that we obtain are consistent with previous determinations.

Differences are noted with previous determinations of the radio luminosity evolution of quasars. Willott et al. (2001) also use a power law parameterization of the radio evolution with redshift for the radio bright sources they consider. Our result for the radio luminosity evolution, when evaluated for the data set as a whole is not consistent to within uncertainty with their results (power laws ranging from 3.1 to 3.6). Strazzullo et al. (2010) have recently obtained results with a radio survey to low (13.5 μ Jy) flux limits, quoting $k_{rad} = 2.7 \pm 0.3$ with the same parameterization used here for the sub-population that they identify as AGN. This is also not in agreement with the radio evolution determined in our analysis.

There has been much discussion as to whether RL and RQ quasars, defined solely by means of the radio loudness parameter as explained above, constitute a true continuum or two populations that can be said to be distinct in some way (e.g. Kellerman et al. (1989); Ivezic et al. (2002); Cirasuolo et al. (2003)). Our analysis favors the former. First, we found that the division of the quasar population into the two aforementioned classes introduces strong biases into the simultaneous determination of the radio and optical luminosity evolutions ($\S4.2$; see also Figure 6). More importantly, as shown in $\S7$, forming a distribution in the raw values of the radio loudness parameter R, without taking into account the biases introduced by the truncations in the data and the correlated luminosity evolutions, results in a shape for the distribution which is very different from the true distribution, and also produces an apparent dip in $G_R(R)$ at $R \sim 10$. By contrast, the true distribution shows at most a modest feature. Even if the feature is real, it does not suggest physically distinct populations, but rather a continuous range of physical properties in a single population.

Accessing the unbiased distribution of the radio loudness parameter for quasar sources is crucial not only for understanding the cosmological evolution of this class of active galaxies, but also for understanding jet launching processes in the vicinities of supermassive black holes. In this context, we note that the observed optical fluxes of quasars are dominated by the emission from an accretion disk accreting at relatively high rates, around 1% - 100%of Eddington, and therefore radiating with $\simeq 10\%$ efficiency. Hence, the optical luminosity is a very good measure of the total accretion power in guasar sources. On the other hand, the observed radio fluxes of the discussed class of objects are expected to originate in the outflowing magnetized plasma. In particular, the radio emission of quasars is produced predominantly via the synchrotron emission of relativistic well-collimated jets (in the case of very radio loud sources), or via the cyclotron and/or free-free emission of at most mildly-relativistic disk winds (in the case of very radio quiet nuclei). In both cases, the observed radio luminosities should be considered as proxies for the kinetic luminosities of the outflowing matter. Therefore, the radio loudness R characterizes the efficiency of the production of jets/outflows for a given accretion power.

The lack of any clear bi-modality in the distribution of the radio loudness parameter for quasars, as advocated here, implies then that there is no critical change in the parameters of the central engine between the radio loud quasars (those producing extremely powerful relativistic jets), and the radio quiet ones (those producing only mildly-relativistic and uncollimated disk winds). This is a crucial piece of evidence for understanding still debated mechanisms for jet launching in active galactic nuclei. Note, for example, that our finding is hardly consistent with the idea for RL quasars to posses counter-rotating (with respect to the black hole spin) accretion disks, as opposed to RQ quasars with co-rotating disks only (Garofalo et al. 2010). Instead, the nuclei of jetted and non-jetted quasar sources — and it has to be emphasized that here we do not discuss the whole population of active galactic nuclei (including, e.g., Seyfert galaxies) but only strictly the guasar population — seem to be intrinsically very similar, differing only smoothly and continuously in some particular respects (see the related recent discussion in Sikora et al. 2007, and references therein).

Another important (and possibly related) result we find is that the radio loudness increases with increasing optical and radio luminosities, as well as with redshift. This implies the existence of some connection between the efficiency of formation of relativistic jets and accretion power, which may in turn depend on the combination of the evolving accretion rate and black hole spin (see in this context Tchekhovskov et al. 2010). Note, however, that even though we have used simple oneparameter functions to describe the emerging correlations, it is possible that some of them are more complex. For example, the correlation index α between the radio and optical luminosities may be close to unity only for low luminosity objects, but much larger than that for more luminous (and therefore radio loud) quasars. More data and further analysis is needed to address this and similar issues, which may provide further constraints on theoretical models.

Another application of the presented analysis is related to the understanding of the origin of the cosmic background radiation in the radio frequency regime. In Singal et al. (2010) we estimated the fractional contribution of quasars to the Cosmic Radio Background, assuming the level reported by Fixsen et al. (2010). In general the flux of the objects fitting the definition of radio loud is well characterized by current interfermoetric radio surveys so that their contribution to the total radio background intensity can be estimated to be 15 to 25 percent of the observed value. In the earlier work we also estimated the total contribution to the background of the radio quiet objects, and found it to be between 1 and 2 percent for favored models of quasar luminosity evolution. This estimate was based on integrating values of the quasar bolometric luminosity function, as reported in the literature, over redshift, applying a mapping between optical and radio luminosity, and assuming that the optical and radio luminosities had identical redshift evolutions. We also noted there that the contribution we estimated was dependent on the later assumption and would be revised in the case of differing radio and optical luminosity evolutions. As we see here that the population of quasars has greater radio evolution relative to optical, the contribution of radio quiet quasars to the radio background will be somewhat larger than the value reported in our previous work. We will present a quantitative determination in a forthcoming paper.

JS thanks S. Kahn and R. Schindler for their encouragement and support. LS was supported by the Polish Ministry of Science and Higher Education through the project N N203 380336.

REFERENCES

- Boyle, B., Shanks, S., Croom, R., Smith, L., Loaring, N. & Heymans, C. 2000, MNRAS, 317, 1014
- Cirasuolo, M., Magliocchetti, A. & Danese, L. 2003, MNRAS, 341.993
- Croom, S., et al. 2009, MNRAS, 399, 1755
- Donoso, E., Best, P., & Kauffmann, G. 2009, MNRAS, 392, 617
- Dunlop, J. & Peacock, J. 1990, MNRAS, 247, 19
- Efron, B. & Petrosian, V. 1992, ApJ, 399, 345 Efron, B. & Petrosian, V. 1999, JASA, 94, 447
- Fixsen D. et al., 2010, ApJ, submitted, preprint (arXiv:0901.0559)
- Garofalo, D., Evans, D. A., & Sambruna, R. M. 2010, MNRAS, 406.975
- Goldschmidt, P., Kukula, M., Miller, L., & Dunlop, J. 1999, ApJ, 511, 612
- Hewett, P., Foltz, C. & Chaffe, F. 2001, ApJ, 122, 518
- Hopkins, P., Richards, G. & Hernquist, L. 2007, AJ, 654, 731
- Hopkins, P., Younger, J., Hayward, C., Narayan, D., & Hernquist, L. 2010, MNRAS, 402, 1693
- Ivezic, Z. et al. 2002, AJ, 124, 2364
- Jiang, L., et al. 2007, aas, 211, 4523
- Kellerman, K., Sramek, R., Schmidt, M., Shaffer, D. & Green, R. 1989, AJ, 98, 1195
- Lynden-Bell, B. 1971, MNRAS, 151, 95
- Maloney, A. & Petrosian, V. 1999, ApJ, 518, 32
- Marshall, H., Tananbaum, H., Avni, Y., & Zamorani, G. 1983, ApJ, 269, 35
- Mauch, T. & Sadler, E. 2007, MNRAS, 375, 931
- Matute, I., LaFranca, F., Pozzi, F., Gruppioni, C., Lari, C & Zamorani, G. 2006, A&A, 451, 443

- Miller, L., Peacock, J., & Mead, A. 1990, MNRAS, 244, 207 Osterbrock, D., 'Astrophysics of Gaseous Gebulae and Active
- Galactic Nuclei ', Mill Valley, CA: University Science Books 1989
- Petrosian, V. 1992, in Statistical Challenges in Modern Astronomy, ed. E.D. Feigelson & G.H. Babu (New York:Springer), 173
- Petrosian, V. 1973, ApJ, 183, 359 Richards, G. et al. 2006, AJ, 131, 2766
- Schmidt, M. 1972, ApJS, 176, 273
- Schmidt, M. 1968, ApJ, 151, 393
- Shaver, P., Wall, J., Kellermann, K., Jackson, C., & Hawkins, M. 1996, Nature, 384, 439
- Singal, J., Stawarz, L., Lawrence, A., & Petrosian, V. 2010, MNRAS, 409, 1172
- Sikora, M., Stawarz, Ł., & Lasota, J.-P. 2007, ApJ, 658, 815
- Strazzullo, V., Pannella, M., Owen, F., Bender, R., Morrison, G, Wei-Hao, W. & Shupe, D. 2010, ApJ, accepted, arXiv:1003.4734
- Tchekhovskoy, A., Narayan, R., & McKinney, J. 2010, ApJ, 711, 50
- Ueda, Y., Akiyama, M., Ohta, K., & Miyaji, T. 2003, ApJ, 598, 886
- White, R. et al. 2000, ApJS, 126, 133
- Willottt, C., Rawlings, S., Blundell, K., Lacy, M., & Eales, S. 2001, MNRAS, 322, 536

Singal et al.

APPENDIX

Distribution of Radio Loudness R: As emphasized in the introduction the proper approach to the main problem of this paper is determination of the distribution of the radio to optical luminosity ratio $R = L_{rad}/L_{opt}$ from an observed sample of radio and optical fluxes and redshifts. Here we show the importance of properly considering the truncations due to selection effects in the data and the correlation in the optical and radio luminosity evolutions.

The true or intrinsic distribution of R values is related to the radio and optical luminosity functions $\Psi(L_{opt}, L_{rad}, z)$ as

$$G_T(R,z) = \int_0^\infty \Psi(L_{opt}, R \ L_{opt}, z) \ L_{opt} \ dL_{opt} = \int_0^\infty \Psi(\frac{L_{rad}}{R}, L_{rad}, z) \ L_{rad} \ \frac{dL_{rad}}{R^2}.$$
 (1)

(compare to the separable, local form in Equation 8)

The observed distribution on the other hand is different because the observational selection effects truncate the data. For example for a sample with well defined flux limits $f_{rad} \ge f_{m,rad}$, $f_{opt} \ge f_{m,opt}$, and $R_{\text{flim}} \equiv f_{m,rad}/f_{m,opt}$ the observed distributions is

$$G_{\rm obs}(R,z) = \int_{L_{\rm min,opt}(z)}^{\infty} \Psi(L_{opt}, R \ L_{opt}, z) \ L_{opt} \ dL_{opt} \quad \text{for} \quad R > R_{\rm flim}$$

$$G_{\rm obs}(R,z) = \int_{L_{\rm min,rad}(z)}^{\infty} \Psi(\frac{L_{rad}}{R}, L_{rad}, z) \ L_{rad} \ \frac{dL_{rad}}{R^2}$$

$$= \int_{L_{\rm min,opt}(z)R_{\rm flim}/\hat{R}}^{\infty} \Psi(L_{opt}, R \ L_{opt}, z) \ L_{opt} \ dL_{opt} \quad \text{for} \quad R < R_{\rm flim},$$

$$(3)$$

where

$$\hat{R} = (K_{opt}/K_{rad})R, \quad L_{\min,opt}(z) = 4\pi d_L^2(z)K_{opt}f_{m,opt} \quad \text{and} \quad L_{\min,rad}(z) = 4\pi d_L^2(z)K_{rad}f_{m,rad}.$$
 (4)

and K_i is the K-correction factor for waveband *i*. All of these are obtained from the observed distributions of the fluxes and redshifts. If we approximate the observed distribution of fluxes and redshifts by a continuous function $n_{\text{obs}}(f_{opt}, f_{rad}, z)$ then

$$\Psi(L_{opt}, L_{rad}, z) = n_{obs} \left(\frac{L_{opt}}{4\pi d_L^2(z) K_{opt}}, \frac{L_{rad}}{4\pi d_L^2(z) K_{rad}}, z \right) \left(\frac{1}{4\pi d_L^2} \right)^2 \frac{1}{K_{opt} K_{rad} V'(z)}$$
(5)

so that

$$G_T(R,z) = (K_{opt}K_{rad}V')^{-1} \int_0^\infty n_{obs}(f_{opt}, \hat{R}f_{opt}, z) f_{opt} df_{opt}$$
(6)

$$G_{\rm obs}(R,z) = (K_{opt}K_{rad}V')^{-1} \int_{f_{lim}}^{\infty} n_{\rm obs}(f_{opt}, \hat{R}f_{opt}, z) f_{opt} df_{opt},$$

$$\tag{7}$$

where V' = dV(z)/dz, and $f_{lim} = f_{m,opt}$ for $\hat{R} > R_{\text{flim}}$ and $f_{lim} = f_{m,opt}(R_{\text{flim}}/\hat{R})$ for $\hat{R} < R_{\text{flim}}$. Note that \hat{R} depends on redshift to the extent that the optical and radio K-corrections are different.

Clearly the observed distribution is different than the true distribution. In reality the situation is more complicated because the lower limit of the integration does not extend to zero. The samples of available quasars are truncated also by minimum luminosities, say $L_{m,opt}$ and $L_{m,rad}$ which introduces a second critical value for R, namely $R_{\text{Llim}} \equiv L_{m,rad}/L_{m,opt}$. The above equations are valid for redsifts $z > z_{\min,\text{rad}}$ defined as

$$L_{m,x} = 4\pi d_L^2(z_{\min,x}) K_i(z_{\min,x}) f_{m,x}.$$
(8)

For $z < z_{\min,opt}$ and/or $z_{\min,rad}$ there is no truncation due to flux limits and $G_{obs} = G_T$.

We now consider different cases with different relative optical and radio flux limits. For convenience we first define

$$\Phi(R, z; x) = \int_{i}^{\infty} \Psi(L_{opt}, R \ L_{opt}, z) \ L_{opt} \ dL_{opt}$$

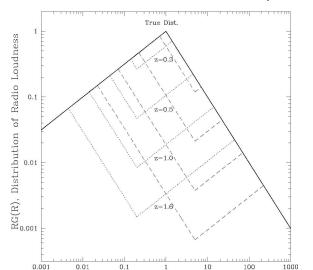
$$\tag{9}$$

so that the true distribution can be written as

$$G_T(R, z) = \Phi(R, z; L_{m,opt}) \quad \text{for} \quad R > R_{\text{Llim}}$$

$$\tag{10}$$

$$G_T(R, z) = \Phi(R, z; \frac{R_{\text{Llim}} L_{m,opt}}{R}) \quad \text{for} \quad R < R_{\text{Llim}}.$$
(11)



Radio Loudnes R=L_5 $_{\rm GHz}/\rm L_{2500~A}$

FIG. 15.— The true distribution in R, $G_T(R, z)$, and the raw observed distributions $G_{obs}(R, z)$, for the simple example highlighted in the text, plotted as $R \times G(R)$ for clarity, with $R_{Llim} = 1$ and $\eta_{opt} = -1.5$ and $\eta_{rad} = -2.5$. The normalization is arbitrary. The solid line is the true distribution, while the dahsed lines show the observed distribution for $R_{flim} = 5$, i.e. a sample that is mostly radio limited observationally, and the dotted lines show the observed distribution for $R_{flim} = 1/5$, is a sample that is mostly optically limited observationally. In this example there is no luminosity evolution so $G_T(R, z)$ has no redshift dependence. Even in this very simplistic model it is seen that the raw observed distribution of R does not match the true one. The truncations inherent in the data give the observer an incorrect observed distribution.

The observed distribution depends on the relative values of $R_{\rm Llim}$ and $R_{\rm flim}$.

Case 1. We first consider a sample where $R_{\text{flim}} > R_{\text{Llim}}$ which means that $z_{\min,\text{rad}} > z_{\min,\text{opt}}$. Such a sample may be classified as *mainly optically selected*. (For purely optically selected sample $R_{\text{flim}} = 0$.) In this case observed distribution will be the same as the true distribution for all redshifts $z < z_{\min,\text{rad}}$. But for higher redsifts $G_T = G_{\text{obs}}$ for

$$R > R_{\max}(z) \equiv L_{\min, \operatorname{rad}}(z) / L_{m, opt} \text{ and } R < R_{\min}(z) \equiv L_{m, rad} / L_{\min, \operatorname{opt}}(z).$$
(12)

In between those two limits the observed distribution is different than G_T ;

$$G_{\rm obs}(R, z) = \Phi(R, z; L_{\rm m, opt}) \quad \text{for} \quad R_{\rm flim} > R > R_{\rm min}(z), \tag{13}$$

$$G_{\rm obs}(R,z) = \Phi(R,z; \frac{R_{\rm flim} L_{\rm m,opt}}{R}) \quad \text{for} \quad R_{\rm max}(z) > R > R_{\rm flim}.$$
(14)

Case 2. In the opposite case of $R_{\text{flim}} < R_{\text{Llim}}$ or $z_{\text{min,rad}} < z_{\text{min,opt}}$ the sample is mainly radio selected and we get similar results but with $z_{\text{min,rad}}$ replaced by $z_{\text{min,opt}}$.

A simple Example: Let us assume that the radio and optical luminosities are uncorrelated and do not evolve so that we have $\Psi(L_{opt}, L_{rad}, z) = \psi_{opt}(L_{opt}) \psi_{rad}(L_{rad}) \rho(z)$, where $\rho(z)$ describes the density evolution. Furthermore if we assume simple power law LFs $\psi_{opt}(L_{opt}) = A_{opt}L_{opt}^{-\eta_{opt}}$ and $\psi_{rad}(L_{rad}) = A_{rad}L_{rad}^{-\eta_{rad}}$, it is easy to show that

$$G_T(R,z) \propto (R/R_{\rm Llim})^{1-\eta_{\rm rad}} \quad \text{for } R > R_{\rm Llim} \quad \text{and} \quad G_T(R,z) \propto (R/R_{\rm Llim})^{\eta_{\rm opt}-1} \quad \text{for } R < R_{\rm Llim}. \tag{15}$$

Similarly it can be shown that by defining and $\beta = \eta_{opt} + \eta_{rad} - 2$ for case 1 we get

$$G_{\rm obs}(R,z) \propto \begin{cases} (R/R_{\rm Llim})^{1-\eta_{rad}} & \text{for } R > R_{\rm max}(z), \\ (R/R_{\rm Llim})^{\eta_{opt}-1} (R_{\rm Llim}/R_{\rm max})^{\beta} & \text{for } R_{\rm flim} < R < R_{\rm max}(z), \\ (R/R_{\rm Llim})^{1-\eta_{rad}} (R_{\rm min}/R_{\rm Llim})^{\beta} & \text{for } R_{\rm min}(z) < R < R_{\rm flim}, \\ (R/R_{\rm Llim})^{\eta_{opt}-1} & \text{for } R < R_{\rm min}(z). \end{cases}$$

In Figure 15 we plot a realization of $G_T(R)$ and $G_{obs}(R)$ for this example. It is clear that even in this extremely simple case the observed and true distributions of the radio loudness R are different, so that the moments of the observed distributions (means and dispersions) could give misleading information, unless the truncations of the data and correlations in the optical and radio luminosities are properly accounted for, as in this work.